La publicació final està disponible a Springer a través: https://doi.org/10.1007/s11307-016-1003-4

Impact of region-of-interest delineation methods, reconstruction algorithms and intra- and inter-operator variability on internal dosimetry estimates using PET

N.López-Vilanova[1,2], J.Pavía[1,3,4], M.A. Duch[2], A.Catafau[4,5], D.Ros[1,4,6], S.Bullich[7]

[1] Centro de Investigación Biomédica en Red en Bioingeniería, Biomateriales y Nanomedicina (CIBER-BBN)

[2] Institut de Tècniques Energètiques (INTE), Universitat Politècnica de Catalunya (UPC)

[3] Nuclear Medicine Dept., Hospital Clínic i Provincial de Barcelona

[4] Institut d'Investigacions Biomèdiques August Pi i Sunyer (IDIBAPS)

[5] Barcelona Imaging Group (BIG)

[6] Unitat de Biofísica i Bioenginyeria, Universitat de Barcelona

[7] Molecular Imaging Centre (CRC-CIM), Barcelona Biomedical Research Park

Correspondence:

N. López-Vilanova

Institut de Tècniques Energètiques (INTE)

Universitat Politècnica de Catalunya (UPC)

Av. Diagonal 647, planta 0, pavelló C

08028 Barcelona, Spain

Tel: +34 93 401 66 92

Email: natalia.lopez-vilanova@gmail.com

Abstract

Purpose: Human dosimetry studies play a central role in PET radioligand development. Drawing regions of interest (ROIs) on the PET images is used to measure the dose in each organ. In the study aspects related to ROI delineation methods were evaluated for two radioligands of different biodistribution (intestinal vs urinary). ***Procedures:*** PET images were simulated from a human voxel-based phantom. Several ROI delineation methods were tested: antero-posterior projections (AP), 3D sub-samples of the organs (S), and a 3D volume covering the whole-organ (W). Inter- and intra-operator variability ROI drawing was evaluated by using human data. ***Results:*** The effective dose estimates using S and W methods were comparable to the true values. AP methods overestimated (49%) the dose for the radioligand with intestinal biodistribution. Moreover, the AP method showed the highest inter-operator variability: 11±1%. ***Conclusions:*** The sub-sampled organ method showed the best balance between quantitative accuracy and inter- and intra-operator variability.

Keywords: PET, dosimetry, [11C]Raclopride, [11C]GSK931145

INTRODUCTION

Estimation of radiation exposure affecting human subjects undergoing positron emission tomography (PET) exploration plays a central role in new radioligand development. Internal dosimetry estimates for each radioligand are essential to calculate the safety limits of injected activity and the maximum number of scans that a subject can undergo. In a diagnostic context, procedures implies the administration of activity levels that do not lead to the appearance of radiation deterministic effects, therefore only stochastic risks have to be considered. However, in any use of ionizing radiation, one must prevent or minimize the risks of the use of the radiation while allowing its beneficial applications. Radiation exposure estimations are, in general, obtained in biodistribution and dosimetry studies where the time course of the radioligand in organs and tissues must be measured. In these kind of studies, multiple whole-body PET scans are acquired after radioligand injection and regions-of-interest (ROIs) placed on the images are used to measure the amount of radioactivity in each organ over time. Time-integrated activity coefficients are then calculated from the time course of the radioligand and are used by software packages such as Olinda/EXM [1] to obtain dosimetry estimates. Olinda/EXM code implements the methods outlined by the Medical Internal Radiation Dose (MIRD) Committee. These doses are estimated based on organ level S values calculated for standard phantoms representing the average male or female. Where S factor is the mean absorbed dose to the target organ, t from unit activity of the relevant radioisotope distributed within the source organ S. The dose is given by summing up the contributions from all source organs. Several methods for delineating regions-of-interest (ROI) and quantification of dosimetry estimates are currently being used. Whole-organ ROI drawn on PET images or on co-registered high-resolution structural images (computed

tomography (CT) or magnetic resonance imaging (MRI)) have been used to estimate the distribution of radioactivity over time [2-3]. However, whole organ ROI delineation is very time-consuming and, as a consequence, simplified methods are also employed. Delineation of ROIs on sub-samples of the organs facilitates ROI drawing, but only activity concentration is obtained with this method together with an approximation of organ volume [4-6]. A further simplification consists of drawing planar ROIs on the antero-posterior compressed images [7-10]. However, delineating and overlapping organs may lead to biased results. There have been several attempts to compare the performance of these methods [10-12]. Nevertheless, the absence of a gold standard with which to compare the dosimetry estimates obtained have made it impossible to draw conclusions about the accuracy of these methods. Additionally, the lack of reliable methods to perform automated organ segmentation makes internal dosimetry estimates operator dependent. To the best of our knowledge, the impact of ROI delineation methods on the inter- and intra-operator variability in internal dosimetry estimates has not been reported to date.

Monte Carlo (MC) simulations are an important tool in the assessment and optimization of image processing methods in nuclear medicine. MC simulations provide an adaptable environment where the ground truth is known and where the realism of the input models can be suitable reproduced. Dedicated MC codes (SimSET, GATE) for PET/SPECT systems, are well-known for its efficiency in the simulation of voxel-based objects [13].

PET image quality, which is related to the reconstruction method used, the corrections for degrading factors applied (randoms, attenuation, scatter, and partial volume) and the number of counts acquired, is another factor to consider in dosimetry studies. Several reconstruction methods, based on the filtered back-projection (FBP) and on the ordered-subsets expectation-maximization (OSEM) algorithm [14] are currently being

used. Corrections such as attenuation, randoms and dead time are routinely applied since they have been shown to increase image quality and quantification accuracy. Scatter correction is also usually applied, but most of the commercial tomographs apply simplified scatter correction methods that only take into account a single scatter correction [15-16]. Although there is extensive literature comparing the performance of both methods in whole-body [17] and brain [18] studies, little is known about their performance in dosimetry studies.

The aim of this study was to evaluate the performance of ROI delineation methods and reconstruction algorithms on the accuracy of internal dosimetry estimates using simulated PET studies for two radioligands with different biodistribution (intestinal and urinary excretion)In addition, the impact of ROI delineation methods on the inter- and intra-operator variability of dosimetry estimates has been assessed using clinical data from a previous study, where a radioligand with intestinal route of clearance was used [12].

MATERIAL AND METHODS

Impact of reconstruction algorithms and ROI drawing on the accuracy of dosimetry estimates

Reference case studies. Two different radioligands with distinct biodistribution and kinetics were simulated ([11C]Raclopride and [11C]GSK931145). The main route of clearance for [11C]Raclopride was urinary, while the principal route of clearance for [11C]GSK931145 was considered to be intestinal. The voxel-based Zubal phantom with arms down [19] was used to generate a realistic anatomical model for subsequent Monte Carlo simulation. The original whole-body phantom was rebinned to a size of 64 x 64 x 200 voxels, with a voxel size of 10x10x10 mm^3. Nine activity models

reproducing the radiotracer concentration in each organ over time were created. Each model reproduced a different time point after injected activity. An homogeneous activity to each organ was assigned using time-activity curves of the simulated radioligands extracted from previously published human PET data [4-5, 12]. Attenuation maps were created from the Zubal phantom segmented into three different tissues: lungs, bone and soft tissue.

PET image simulations. PET acquisitions were simulated using SimSET [20] Monte Carlo code (version 2.9) (http://depts.washington.edu/simset), which was configured for a General Electric Discovery ST PET/CT scanner [21]. The detector was modeled as a single ring of bismuth germanate (BGO) material. The energy window was 375-650 keV and simulations were performed in 3D. The output sinograms covered a 15.7cm axial field of view (FOV). The number of transaxial and angular bins were 128 and 140, respectively and 192 was the number of axial slices (1 cm slice size) [22]. Eight bed positions each corresponding to the dimension of the scanner axial FOV were independently simulated to achieve whole-body coverage. An overlap of 1.3 cm (corresponding to 4 slices) was considered between two consecutive bed positions to compensate for the loss of sensitivity on both extremities of the axial FOV. To realistically simulate the noise levels in dynamic PET studies, firstlynoise-free sinograms (noise in simulations was 100 times less than noise obtained in real acquisitions) were scaled to have the same number of counts as in a clinical scan [23].Secondly, Poisson distribution noise was added to each of them to mimic the number of counts collected per frame in realistic dynamic PET studies. True coincidences, single scatter coincidences and multiple scatter coincidences were stored in separate files to assess the effect of Compton scatter. Then standard PET corrections were made [24].Two different scatter correction methods were applied on the

sinogram: a) an ideal scatter correction (ISC) which considered only true coincidences on the sinograms [25] and b) ideal single scatter correction by subtracting Monte Carlo simulated single scatter coincidences from the sinograms. Attenuation correction and rebinning were performed on the sinograms for the true coincidences before reconstruction.

Reconstruction algorithms. STIR [26] was employed to reconstruct the data using three different methods (http://stir.sourceforge.net/): a) 2D Filtered back projection (FBP 2D) (transaxial filter: ramp, cut-off: 0.2 cycles), b) 3D Filtered back projection (FBP 3D): 3D re-projection (transaxial filter: ramp, cut-off frequency: 0.2 cycles; axial filter: Colsher, cut-off frequency: 0.5 cycles) and c) Ordered-subset expectation-maximization (OSEM): number of subsets: 5; number of iterations: from 1 to 20. The resulting images consisted of nine frames of volumes of the size 128 x 128 x 47 mm^3. The voxel size was 5.47 x 5.47 x 3.34 mm^3.

Calibration factor estimation. Activity units were obtained after calibration using a SimSET Monte Carlo simulation of an homogeneous cylindrical phantom with the same parameters as those used for the simulation of the dosimetry study. A calibration factor was obtained for the reconstruction algorithms applied.

Impact of inter- and intra- operator variability of ROI drawing on the precision of dosimetry estimates

Clinical human data. Inter- and intra-operator variability of the different methods to obtain dosimetry estimates was evaluated using clinical data acquired in an earlier study [12]. In such study, eight healthy human volunteers (4 M /4 F) underwent whole-body PET/CT scans on a General Electric Discovery ST scanner which used a 3-dimensional mode protocol. A CT scan (80 mA, 120 keV) was acquired before tracer

injection and used for subsequent attenuation correction and reconstructed to generate 512×512×593 voxel volumes (0.98×0.98×1.80 mm^3). Emission scans were acquired after intravenous injection of a 1-min bolus of the ^{11}C-GSK931145 radioligand followed by 30-s flushing with saline. Emission scans were collected in nine passes of increasing duration (15, 15, 30, 30, 60, 60, 120, 180, and 240 s per bed) with six to seven overlapping bed positions from the head to the mid-thigh of the subject. PET data were reconstructed using a OSEM reconstruction algorithm which included correction for attenuation, scatter, randoms and dead time to generate 128×128×327 voxel volumes (3.91×3.91×3.27 mm^3). For activity quantification in PET planar images and according to previous works, there were no background susbstraction. In such studies it was demonstrated that analysis of compressed planar images were comparable to tomographic images, but with a slight overestimation (conservative calculation) [8-9, 11-12].

Calibration factor estimation. A homogeneous water-filled phantom with a known concentration of ^{18}F was used to determine the cross-calibration factor between PET and the dose calibrator. This factor was applied to the PET data to generate quantitative images.

Assessment of inter- and intra- operator variability. The three delineation procedures which are detailed in II.C. were used by six (for AP and S methods) and five (for W method) independent operators on all subjects to examine inter-operator variability. Additionally, two of the operators carried out the procedures twice to examine intra-operator variability.

The intra- and inter-operator variability in effective doses (ED) was calculated as the mean variability of the standard deviation of the ED calculated by all operators. Estimation of the uncertainty of the variability for the three delineation methods was

provided. Similar calculations were done to estimate the percentage of variability of the absorbed doses (AD).

II.B.3.1. Statistical analysis. Human data were analyzed using two-way analysis of variance (ANOVA) to test differences in the ED values using operator and methods of ROI delineation as factors. When the overall F statistic was significant, post-hoc comparison of ROI methods using the Scheffé approach was performed. A probability threshold of 0.05 was chosen as the significance level. Statistical analysis system (SAS) 9.2 for Windows was used for statistical analysis.

Delineation methods

Dosimetry was estimated by using three ROI delineation methods differing in their complexity and execution time. ROIs were drawn on the following organs: brain, heart, lungs, stomach, liver, gallbladder, intestine, kidneys, urinary bladder and cortical bone, using MRIcro software [27]. For planar images, the user draws a region on the image by using the available MRIcro tools. In 3D methods, the drawing is performed on each slice encompassing the volume of interest and the set of resulting regions are then combined to form a 3-D volume [28]. These ROIs were drawn in three different ways:

Antero-posterior compressed images (AP). Images were compressed by projecting the reconstructed images in the antero-posterior direction to obtain planar images. ROIs were drawn on the planar images (one single slice) covering the entire organ; it was done six times due to the variability expected using this method. Results were expressed as the mean value and the uncertainty in the mean.

Sub-sample of the organs (S). Spherical ROIs were applied on 3D images and only the center and radius of the ROI were fixed interactively using the graphical interface. For reference simulated data, ROIs were scaled according to the organ volumes

derived from Zubal phantom and a same operator have drawn ROIs three times. Results were expressed as the mean value and and the uncertainty in the mean. In addition, to assess the variability of the results on organ size, variations within ±20% in organ volumes were applied from the anatomical regions of the Zubal phantom. For clinical human data, ROIs were scaled according to the organ volumes derived from adult (male and female) numerical phantoms [29].

Whole-organ (W). For reference simulated data, we considered (i) the optimal case using ROIs obtained from the anatomical regions of the Zubal phantom and (ii) to assess the variability of the results on organ size, variations within ±20% in organ volumes were applied from the anatomical regions of the Zubal phantom. For clinical human data, ROIs were drawn on the CT encompassing the whole-organ, following each organ shape, with the exception of the cortical bone, red marrow, and small and large intestine ROIs, which were drawn only in sub-samples of the organs as described above. All the ROIs drawn on the CT images were verified by overlapping the ROIs on the PET images. Organ volumes considered were derived from CT subjects.

Time-integrated activity coefficients and Absorbed Dose Calculations. ROIs delineated using the methods described in the previous section were applied to the PET images to obtain time-activity curves. The area under the non-corrected time-activity curves (TACs) was calculated with the trapezoidal method of integration [24]. To be conservative, we calculated the area under the curve from the final data acquisition to infinity by assuming that decline in radioactivity occurred only by physical decay. The area under the time-activity curve of the source organ from time zero to infinity divided by the injected activity is equivalent to the time-integrated activity coefficient ($\tilde{a}(r_s, T_D)$). The $\tilde{a}(r_s, T_D)$ for all the source organs was summed and subtracted from

the true total time-integrated activity coefficient value ($T_{1/2}$/ln 2 = 0.49 h) to calculate the ã (r_s, T_D) of the remainder of the body ($T_{1/2}$: the radioactive half-life of [11C]).

Time-integrated activity coefficients were inputted into OLINDA/EXM (version 1.0) software[1] and a 70kg adult male and a 55kg adult female phantom were used to obtain both organ AD and ED.

Reference dose estimations. Reference TACS from the considered studies [4-5, 12] were also inputted into OLINDA/EXM to obtain the true dosimetry estimates for comparison purposes.

RESULTS

ROI method comparison on simulated PET images. Fig. 1 shows transverse slices of the resulting images over time, showing the biodistribution and routes of excretion of [11C]Raclopride and [11C]GSK931145. As we have already pointed out, both biodistributions simulated high activity in the liver for early scans. As expected activity in the contents of the stomach and small intestine was present in [11C]GSK931145 biodistribution where the simulated route of clearance was intestinal. Activity in the urinary bladder was present in [11C]Raclopride biodistribution simulating urinary excretion.

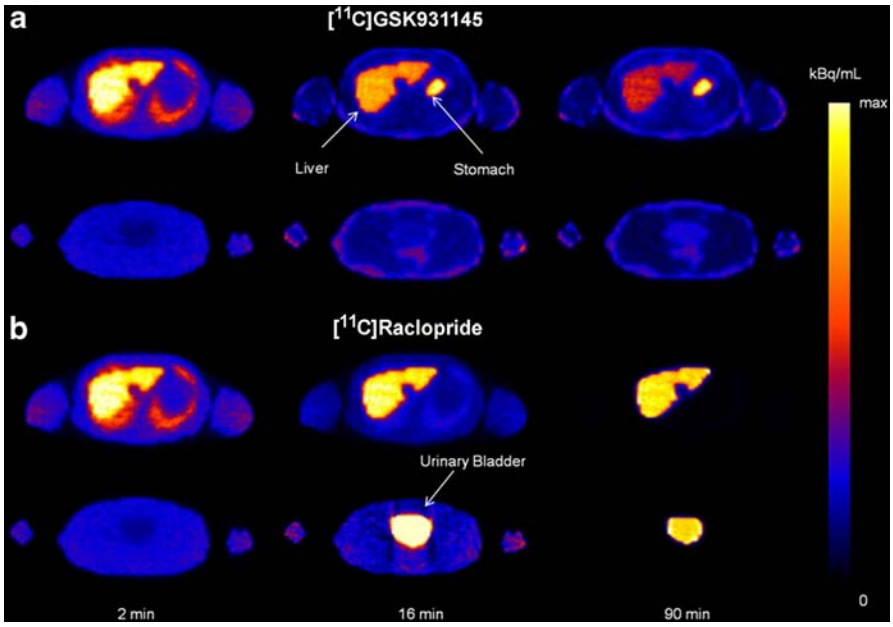

Fig. 1 Illustative transverse slices showing the simulated biodistribution of a [^{11}C]GSK931145 and b [^{11}C]raclopride (*bottom*) in whole-body PET images at 2, 16, and 90 min after injection of the radioligand. For each radioligand, two slices at the level of the liver and urinary bladder are shown. Images reconstructed using OSEM and ISC.

Reconstruction. Effective dose estimates using images reconstructed using OSEM increased their value when the number of iterations was increased until a plateau was reached after approximately 15 iterations. Using the W ROI delineation method for the [11C]GSK931145 distribution, no differences in ED estimates were found when OSEM, FBP 2D and FBP 3D were applied (Fig. 2). The same pattern was found when S and AP ROI delineation methods were applied.

No significant differences (less than 1%) were found in ED estimates when using full scatter correction and single scatter correction.

For the sake of simplicity, from now onwards, results are referred to simulated PET images reconstructed using FBP 2D algorithm and ideal scatter correction.

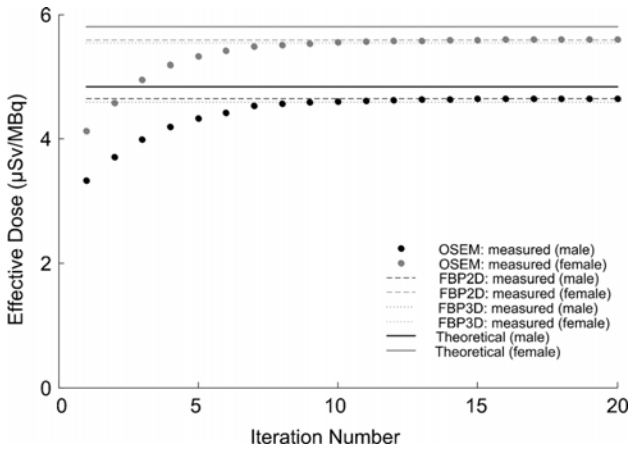

Fig. 2 Comparison of the reconstruction algorithm applied: FBP2D, FBP3D, and OSEM with five subsets and from 1 to 20 iterations, which corresponds to positions 1 to 20 on the *x*-axis. Values are the effective dose estimates for the [^{11}C]GSK931145 distribution whole-body ROI delineation method.

Delineation methods. Measured and true TACs showed close agreement when S and W ROI delineation methods were used. When the AP method was used, measured TACs presented higher activity than simulated TACs in those organs where the ROI enclosed the whole organ (heart, lungs and liver) (Fig. 3).

However, lower activity in the TACs in comparison with the simulated ones was found for the AP method for those organs where only a portion of the organ was delineated (kidneys and intestine) due to overlapping between organs. A similar pattern was found in the time-integrated activity coefficient and absorbed dose where S and W were comparable to the true values and AP methods showed differing results depending on how the ROIs were drawn due to overlapping between organs (Fig. 4 and Fig. 5). As expected, higher TACs lead to higher $\tilde{a}$ (r_s, T_D) and dose estimations.

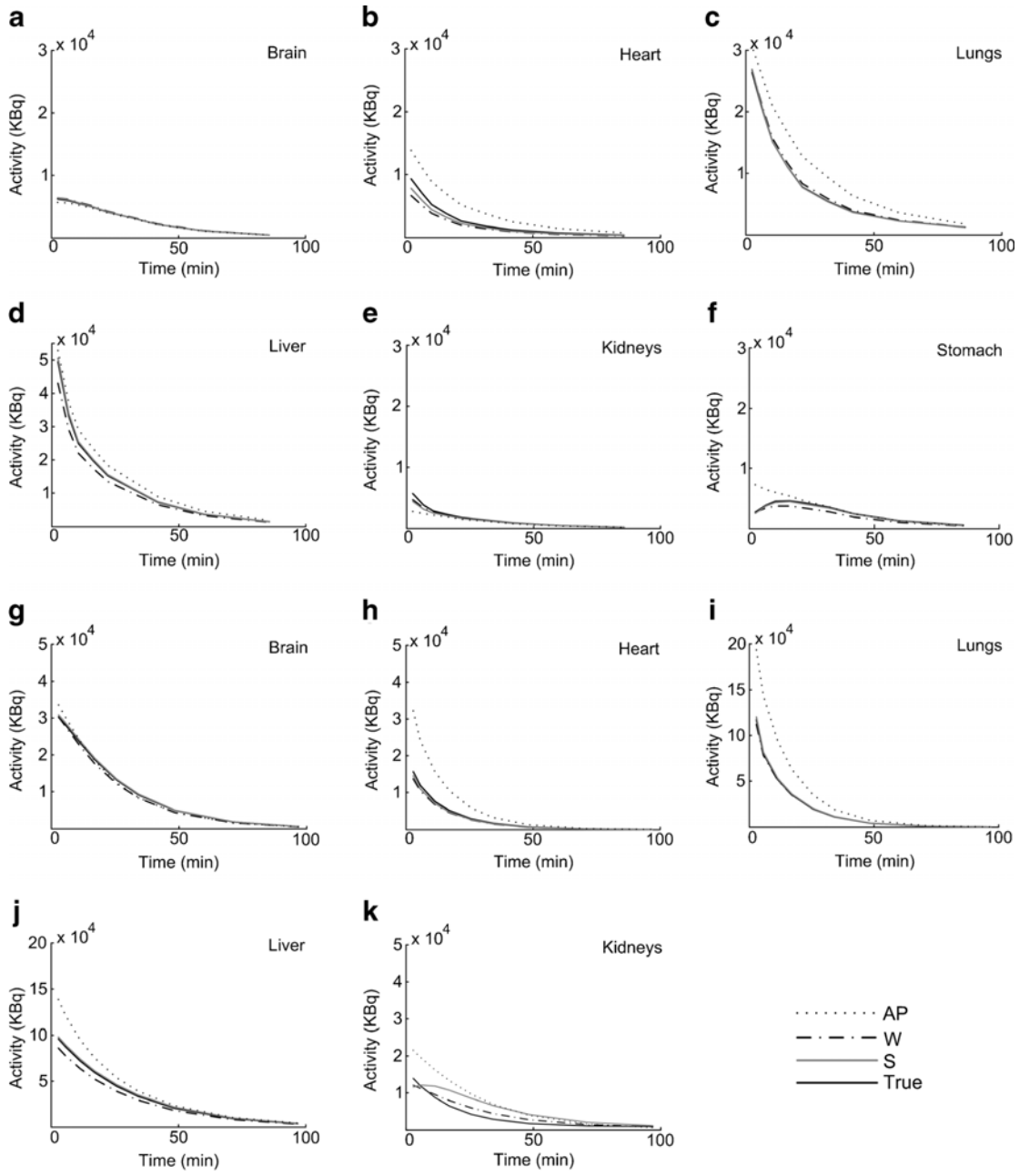

Fig. 3 Simulated and true time-activity curves using different ROI delineation methods (*AP* antero-posterior, *S* subsamples, *W* whole body) of some representative organs for a–f [^{11}C]GSK931145 and g–k [^{11}C]raclopride. Images reconstructed using FBP2D and ISC.

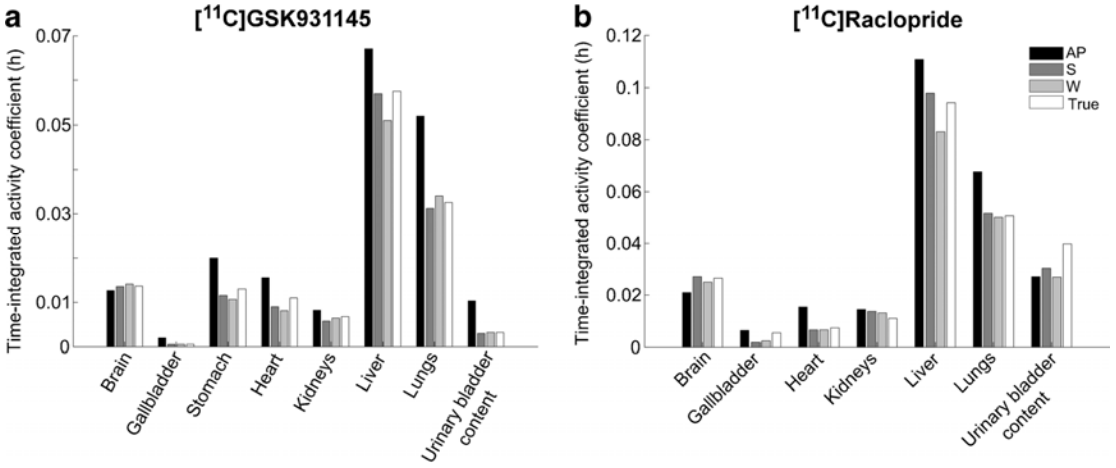

Fig. 4 Time-integrated activity coefficient (ã (rs, TD)) for a [^{11}C]GSK931145 and b [^{11}C]raclopride distributions. ã (rs, TD) calculated from 2D planar images (AP ROI method applied) and tomographic (3D) images (S and W ROI methods applied).

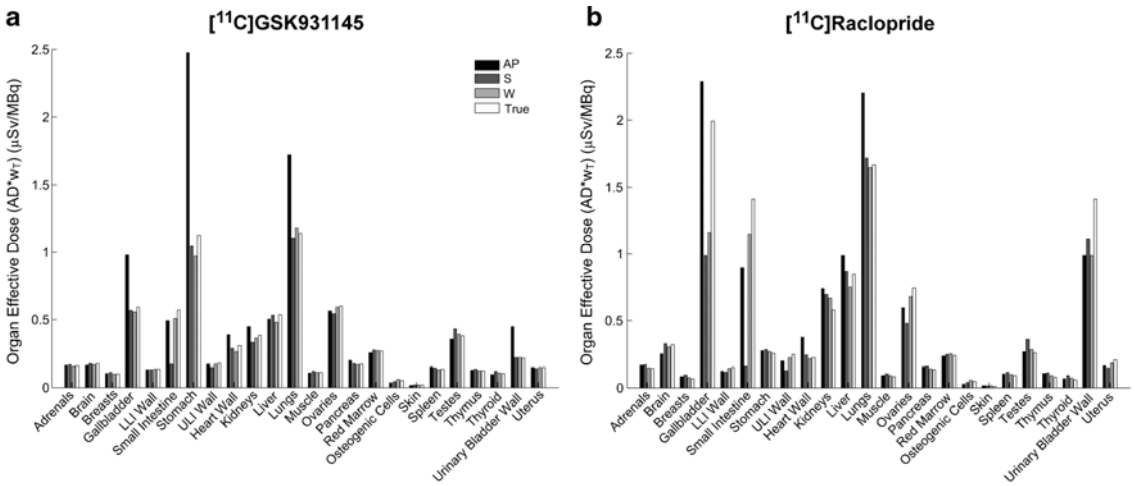

Fig. 5 Comparison of the organ-effective doses (μSv/MBq) using different ROI delineation methods (AP, S, and W) for a [^{11}C]GSK931145 and b [^{11}C]raclopride distributions.

For both simulated radioligands, effective dose estimates using S and W methods showed close agreement with true values ([11C]GSK931145: 4.8 μSv/MBq (true), 4.6 μSv/MBq (W), 4.5±0.5 μSv/MBq (S); [11C]Raclopride: 6.0 μSv/MBq (true), 5.8

μSv/MBq (W), 5.4±0.2 μSv/MBq (S)) (Table 1). For [11C]GSK931145 radioligand, ROIs drawn on AP compressed images provided higher effective dose estimates than true values and the S and W ROI delineation methods (4.8 μSv/MBq (true), 6.7±0.5 μSv/MBq (AP)). For [11C]Raclopride, true effective dose was higher than the similar values provided by the three delineation methods: 6.0 μSv/MBq (true), 6.1±0.3 μSv/MBq (AP)). The organs with the highest tissue-weighted (w_t were taken from ICRP Publication 60) absorbed dose and ED were the lungs and the liver. The estimations obtained with the S and W methods showed good agreement with the true values (Table 1). The AP method provided higher values in ED and AD in the lungs and liver in comparison with the true value (Table 1). Considering a real situation including errors on organ volume estimates, errors up to ±20% of the organ size when using the S method for [11C]Raclopride lead to errors in the ED of up to ±10% (Fig. 6). Men and women showed the same pattern. Nevertheless, women's dose estimations were on average 22% higher than men's results.

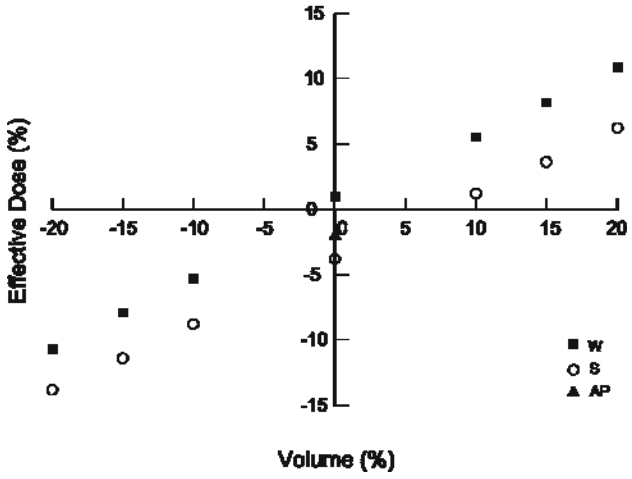

Fig. 6 Percentage difference of effective dose from the whole-organ method for [^{11}C]raclopride distribution using different organ volumes.

Table 1 Radiation-absorbed dose (AD) and effective dose (ED) estimates using different ROI delineation methods (AP, S and W)

	[11C]GSK931145				[11C]Raclopride			
	True	AP	S	W	Theor.	AP	S	W
Liver AD (μSv/MBq)	10.7	10.0±1.8	10.6±0.2	9.59	16.9	19.7±0.9	17.3±0.1	15.0
Lung AD (μSv/MBq)	9.5	14.4±1.8	9.2±1.7	9.82	13.9	18.3±1.9	14.3±0.1	13.7
Stomach AD (μSv/MBq)	9.4	20.6±4.9	8.7±0.2	8.07	2.1	2.3±0.1	2.4±0.1	2.2
ED (μSv/MBq)	4.8	6.7±0.5	4.5±0.5	4.64	6.0	6.1±0.3	5.4±0.2	5.8

Inter- intra- operator variability. Variance analysis presented significant differences in mean dosimetry estimates depending on the delineation method ($p<0.001$). Post hoc analysis showed significant differences in the effective dose between the AP method

and the other two methods studied (S and W). However, there were no differences between S and W. No significant differences were also found between the effective dose measured by different operators. The three delineation methods showed the same intra-operator variability in the effective ED estimates. AP method showed higher intra-operator variability in the AD estimates than the S and W methods (Table 2 and Table 3). AP also showed higher inter-operator variability in the ED estimates and AD estimates than the S and W methods (Table 2 and Table 3). Inter-operator variability was slightly reduced in the case that both operators delineated ROIs according to same criteria.

Table 2 Inter- and intra-operator percentage variability

	Method	Variability (intra-operator)	Variability (inter-operator)
ED (μSv/MBq)	AP	4 ± 1 %	11 ± 1 %
	S	4 ± 1 %	4 ± 1 %
	W	4 ± 1 %	5 ± 1 %

Table 3 Inter- and intra-operator percentage variability

	Method	Variability (intra-operator)	Variability (inter-operator)	
			AD (μGy)	$AD \times W_T$[a] (μGy)
Liver (W_T=0.05)	AP	12 ± 6 %	12 ± 3%	0.6%
	S	8 ± 5 %	8 ± 3%	0.4%
	W	3 ± 1 %	3 ± 1 %	0.2%
Lungs (W_T=0.12)	AP	13 ± 5 %	18 ± 3 %	2%
	S	15 ± 9%	15 ± 7%	2%
	W	11 ± 6%	11 ± 6%	1%
Stomach (W_T=0.12)	AP	14 ± 5 %	31 ± 2%	4 %
	S	11 ± 3 %	15 ± 3%	2%
	W	7 ± 2%	7 ± 2%	1%

[a]Tissue weighting factor

DISCUSSION

Reconstruction. OSEM provided closer ED estimates to the simulated ones. However, the influence of reconstruction algorithms was minimal. This can be explained by the fact that in dosimetry studies not only is the relative contrast between structures important, but also the global activity distributed on organs. An activity calibration method for each reconstruction algorithm is an important step to obtain images providing accurate global activity estimates. Additionally, the absorbed dose received by an organ has a contribution from distant organs, thus in terms of calibration of the global mean activity, differences in contrast have a lower effect. Furthermore, large ROIs encompassing complete organs used in dosimetry contribute to reduce the impact that the partial volume effect may have on the images [30]. A similar argument could be used for the lack of differences found when using full scatter correction and single scatter correction. Full scatter correction is, in theory, more accurate than single scatter correction. However, the calibrated activity used for dosimetry estimations provides an accurate mean global distribution which leads to accurate ED estimates.

ROI delineation comparison. In this study 2D planar image analyses (AP) and two 3D ROI delineation methods (S and W) for obtaining time-activity curves were compared using PET simulated images as the gold standard. The differences in the ED obtained were small between 3D methods, as it would be expected when taking into account organs of the same volume. However, there is a slight underestimation of the ED in comparison with the true value. For [11C]GSK931145 radioligand, with intestinal route of excretion, planar methods overestimate due to a combination of delineating, overlapping between ROIs (mainly for lungs and stomach) and the background activity in the planar projection view. The fact that these differences were not found for

[11C]Raclopride radioligand could be attributed to the route of excretion, since the involved organs reduce the impact of errors related to delineation and overlapping on the effective dose. The same behavior would be expected for radioligands with the same biodistribution and route of excretion. Delineation of whole-organ ROIs was considerably more time-consuming in large organs since the ROIs were drawn manually on the whole set of transverse slices of the CT including the complete organ by following its anatomical contours (~6 h per subject). Analysis time for estimating radiation dose can be shortened by using sub-samples of the organ or delineating ROIs on 2D compressed images. The time spent drawing ROIs on the AP compressed images and on sub-samples of the organs was similar (~15 min per subject). In the AP method, each ROI was drawn on the AP compressed image (one single slice). For the sub-sampled organ method, spherical ROIs were applied on 3D images and only the center and radius of the ROI were fixed interactively using a graphical interface, which substantially simplifies the method (~15 min per subject).

It was observed that ED estimations were sensitive to whichever delineation ROI method was applied. The difficulty lies in delineating the border of each region with precision, whether excluding or not blurred borders in the forming ROIs. Thus, slight differences in boundary delineation have a great effect on dose estimations. The AP method showed the highest inter-operator variability, in particular, the highest organ doses were obtained when including the blurred borders, and the corresponding ED were overestimated. The purpose of this study was to evaluate the impact of ROI delineation methods on accuracy and precision of dosimetry estimates. The next step would be the evaluation of the errors associated[30] to the use of using phantoms instead of performing an individual dosimetry, however, in diagnostic applications, using a phantom instead of a patient-specific model seems to be acceptable. In

therapeutic applications, however the model-based dosimetry would not be appropriate and it would be better use a patient-specific modelling.

Inter- intra- operator variability. Inter operator variability results showed higher reproducibility of the three dimensional methods in comparison with two dimensional methods. The S method was substantially less time consuming and showed comparable inter- and intra-operator variability compared with the W method and may provide the best option in the balance between analysis time, accuracy and reproducibility. Nevertheless, care should be taken when using the S method since errors in the organ volume estimation may have an impact on the effective dose estimates [31-32]. This is the case of subjects that are quite different from the phantom used by Olinda/EXM. In these cases, whole organ ROIs would be desirable. Although some investigators have claimed that the 2D approach is the method of choice because of its considerable ease and conservative estimate of radiation burden, it does not appear to be the optimal method for individual dosimetry estimates of ligands due to its high inter- and intra-operator variability. This large variability is likely to be due to volume delineation.

CONCLUSIONS

Among the three methods compared to draw ROIs, the sub-sampled organ method showed the best balance between quantitative accuracy, inter- and intra-subject variability and practical implementation. Similar quantitative accuracy can be found with either FBP (2D and 3D) or OSEM reconstruction methods.

Acknowledgments. This work was supported in part by the Fondo de Investigación Sanitaria (FIS) of the Instituto de Salud Carlos III under Grant PI12/00390, the CDTI

as part of the CENIT Program (AMIT Project), and the Spanish Ministry of Economy and Competitiveness under Project No. SAF2009-08076. The work of N.López-Vilanova was supported by a research contract from the *Centro de Investigación Biomédica en Red en* Bioingeniería, Biomateriales y Nanomedicina *(CIBER-BBN)*.
MA.D. also express her gratitude to the Grup Consolidat 2014SGR846 from the Spanish Generalitat de Catalunya

Conflict of interest. The authors declare that they have no conflict of interest.

Ethical approval. All procedures performed in studies involving human participants were in accordance with the ethical standards of the institutional and/or national research committee and with the 1964 Helsinki declaration and its later amendments or comparable ethical standards.

Informed consent. Informed consent was obtained from all individual participants included in the study.

REFERENCES

1. Stabin MG, Sparks RB, Crowe E (2005) OLINDA/EXM: the second generation personal computer software for internal dose assessment in nuclear medicine. J Nucl Med 46:1023–1027

2. Bélanger MJ, Simpson NR, Wang T et al (2004) Biodistribution and radiation dosimetry of [11C]DASB in baboon. Nucl Med Biol 31:1097–1102

3. Van Laere K, Koole M, Sanabria Bohorquez SM et al (2008) Whole body biodistribution and radiation dosimetry of the human cannabinoid type-1 receptor ligand 18F-MK-9470 in healthy subjects. J Nucl Med 49:439–445

4. Slifstein M, Hwang DR, Martinez D et al (2006) Biodistribution and radiation dosimetry of the dopamine D2 ligand 11C-Raclopride determined from human whole-body PET. J Nucl Med 47:313–319

5. Ribeiro MJ, Ricard M, Bourgeois S et al (2005) Biodistribution and radiation dosimetry of [11C]raclopride in healthy volunteers. Eur J Nucl Med Mol Imaging 32:952–958

6. Scheinin NM, Tolvanen TK, Wilson IA et al (2007) Biodistribution and radiation dosimetry of the amyloid imaging agent 11C-PIB in humans. J Nucl Med 48:128–133

7. Brown AK, Fujita M, Fujimura Y et al (2007) Radiation dosimetry and biodistribution in monkey and man of 11C-PBR28: a PET radioligand to image inflammation. J Nucl Med 48:2072–2079

8. Cropley VL, Fujita M, Musachio JL et al (2006) Whole-body biodistribution and estimation of radiation-absorbed doses of the dopamine D1 receptor radioligand 11C-NNC 112 in humans. J Nucl Med 47:100–104

9. Lu JQ, Ichise M, Liow JS et al (2004) Biodistribution and radiation dosimetry of the serotonin transporter ligand 11C-DASB determined from human whole-body PET. J Nucl Med 45:1555–1559

10. Sprague DR, Fujita M, Hoon Ryu Y et al (2008) Whole-body distribution and radiation dosimetry in monkeys and humans of the phosphodiesterase 4 radioligand [11C](R)-rolipram: comparison of two-dimensional planar, bisected and quatrisected image analyses. Nucl Med Biol 35:493–500

11. Tipre DN, Lu JQ, Fujita M et al (2004) Radiation dosimetry estimates for the PET serotonin transporter probe 11C-DASB determined from whole-body imaging in non-human primates. Nucl Med Commun 25:81–86

12. Bullich S, Slifstein M, Passchier J et al (2011) Biodistribution and radiation dosimetry of the Glycine Transporter-1 Ligand ^{11}C-GSK931145 Determined from Primate and Human Whole-Body PET. Mol Imaging Biol 13(4):776-784

13. Papadimitroulas P, Loudos G, Le Maitre A et al (2013) Investigation of realistic PET simulations incorporating tumor patient's specificity using anthropomorphic models: creation of an oncology database. Med Phys 40 (11): 112506

14. HM Hudson, RS Larkin (1994) Accelerated image reconstruction using ordered subsets of projection data. IEEE Trans Med Imaging 13(4):601–609

15. JM Ollinger (1996) Model-based scatter correction for fully 3D PET. Phys Med Biol 41:153–176

16. CC Watson (2000) New, faster, image-based scatter correction for 3D PET. IEEE Trans Nucl Sci 47(4):1587–1594

17. El Fakhri G, Santos PA, Badawi RD et al (2007) Impact of acquisition geometry, image processing, and patient size on lesion detection in whole-body 18F-FDG PET. J Nucl Med 48(12):1951-1960

18. Reilhac A, Tomeï S, Buvat I et al (2008) Simulation-based evaluation of OSEM iterative reconstruction methods in dynamic brain PET studies. Neuroimage 39(1):359-368

19. Zubal IG, Harrell CR, Smith EO et al (1994) Computerized 3-dimensional segmented human anatomy. Med Phys 21:299-302

20. Harrison RL, Vannoy SD, Haynor DR et al (1993) Preliminary Experience with the Photon History Generator Module of a Public-Domain Simulation System for Emission Tomography. Records of IEEE Nuclear Science Symposium and Medical Imaging Conference 1154-1158

21. Haynor DR, Harrison RL, Lewellen TK (1994) The use of importance sampling techniques to improve the efficiency of photon tracking in emission tomography simulations. Med Phys 18(5):990–1001

22. Zhu X, El Fakhri G (2009) Monte Carlo modeling of cascade gamma rays in 86Y PET imaging: Preliminary results. Phys Med Biol 54(13):4181-93

23. Aguiar P (2008) Reconstruction, quantification and standardization methods in Positron Emission Tomography. Dissertation, Universitat de Barcelona

24. Siegel JA, Thomas SR, Stubbs JB et al (1999) MIRD Pamphlet No. 16: Techniques for qulantitative radiopharmaceutical biodistribution data acquisition and analysis for use in human radiation dose estimates. J Nucl Med 40: 37S-61S

25. Thielemans K, Manjeshwar RM, Tsoumpas Ch et al (2007) A new algorithm for scaling of PET scatter estimates using all coincidence events. IEEE Nuclear Science Symposium Conference Record 5:3586-3590

26. Thielemans K, Tsoumpas C, Mustafovic S et al (2012) STIR: Software for Tomographic Image Reconstruction Release 2. Phys Med Biol 57 (4): 867-883

27. Rorden C, Brett M (2000) Stereotaxic display of brain lesions. *Behav Neurol* 12:191–200

28. IAEA Human Health Reports No. 9 (2014) Quantitative Nuclear Medicine imaging: Concepts, Requirements and Methods

29. Cristy M, Eckerman K (1987) Specific Absorbed Fractions of Energy at Various Ages from Internal Photon Sources. *Oak Ridge, TN: Oak Ridge National Laboratory*

30. Lassmann M, Chiesa C, Flux G et al (2011) EANM Dosimetry Comitee guidance document: good practice of clinical dosimetry reporting. Eur J Nucl Med Mol 38:192-200

31. Na YH, Zhang B, Zhang J et al (2010) Deformable adult human phantoms for radiation protection dosimetry: anthropometric data representing size distributions of adult worker populations and software algorithms. Phys Med Biol 55:3789–3811

32. Clark LD, Stabin MG, Fernald MJ et al (2010) Changes in Radiation Dose with Variations in Human Anatomy: Moderately and Severely Obese Adults. J of Nucl Med 51(6): 929-932